


RESEARCH ARTICLES

Open Access



# Precision of CT-derived alveolar recruitment assessed by human observers and a machine learning algorithm in moderate and severe ARDS

Ludmilla Penarrubia<sup>1†</sup>, Aude Verstraete<sup>2†</sup>, Maciej Orkisz<sup>1</sup>, Eduardo Davila<sup>1</sup>, Loic Boussel<sup>1,3</sup>, Hodane Yonis<sup>2</sup>, Mehdi Mezidi<sup>2</sup>, Francois Dhelft<sup>2,4</sup>, William Danjou<sup>2</sup>, Alwin Bazzani<sup>2</sup>, Florian Sigaud<sup>5</sup>, Sam Bayat<sup>6,7</sup>, Nicolas Terzi<sup>8,9,10</sup>, Mehdi Girard<sup>2</sup>, Laurent Bitker<sup>1,2</sup>, Emmanuel Roux<sup>1</sup> and Jean-Christophe Richard<sup>1,2\*</sup> 

<sup>†</sup>Ludmilla Penarrubia and Aude Verstraete equally contributed to the manuscript

\*Correspondence:  
[j-christophe.richard@chu-lyon.fr](mailto:j-christophe.richard@chu-lyon.fr)

<sup>2</sup> Service de Médecine Intensive Réanimation, Hôpital de la Croix Rousse, Hospices Civils de Lyon, 103 Grande Rue de La Croix Rousse, 69004 Lyon, France  
Full list of author information is available at the end of the article

## Abstract

**Background:** Assessing measurement error in alveolar recruitment on computed tomography (CT) is of paramount importance to select a reliable threshold identifying patients with high potential for alveolar recruitment and to rationalize positive end-expiratory pressure (PEEP) setting in acute respiratory distress syndrome (ARDS). The aim of this study was to assess both intra- and inter-observer smallest real difference (SRD) exceeding measurement error of recruitment using both human and machine learning-made lung segmentation (i.e., delineation) on CT. This single-center observational study was performed on adult ARDS patients. CT were acquired at end-expiration and end-inspiration at the PEEP level selected by clinicians, and at end-expiration at PEEP 5 and 15 cmH<sub>2</sub>O. Two human observers and a machine learning algorithm performed lung segmentation. Recruitment was computed as the weight change of the non-aerated compartment on CT between PEEP 5 and 15 cmH<sub>2</sub>O.

**Results:** Thirteen patients were included, of whom 11 (85%) presented a severe ARDS. Intra- and inter-observer measurements of recruitment were virtually unbiased, with 95% confidence intervals (CI<sub>95%</sub>) encompassing zero. The intra-observer SRD of recruitment amounted to 3.5 [CI<sub>95%</sub> 2.4–5.2]% of lung weight. The human–human inter-observer SRD of recruitment was slightly higher amounting to 5.7 [CI<sub>95%</sub> 4.0–8.0]% of lung weight, as was the human–machine SRD (5.9 [CI<sub>95%</sub> 4.3–7.8]% of lung weight). Regarding other CT measurements, both intra-observer and inter-observer SRD were close to zero for the CT-measurements focusing on aerated lung (end-expiratory lung volume, hyperinflation), and higher for the CT-measurements relying on accurate segmentation of the non-aerated lung (lung weight, tidal recruitment...). The average symmetric surface distance between lung segmentation masks was significantly lower in intra-observer comparisons (0.8 mm [interquartile range (IQR) 0.6–0.9]) as compared to human–human (1.0 mm [IQR 0.8–1.3]) and human–machine inter-observer comparisons (1.1 mm [IQR 0.9–1.3]).

**Conclusions:** The SRD exceeding intra-observer experimental error in the measurement of alveolar recruitment may be conservatively set to 5% (i.e., the upper value of the  $CI_{95\%}$ ). Human–machine and human–human inter-observer measurement errors with CT are of similar magnitude, suggesting that machine learning segmentation algorithms are credible alternative to humans for quantifying alveolar recruitment on CT.

**Keywords:** Acute respiratory distress syndrome, Computed tomography, Alveolar recruitment, Bias, Repeatability, Reproducibility, Measurement error, Machine learning

## Background

Quantitative computed tomography (CT) has been extensively used to study acute respiratory distress syndrome (ARDS) morphology and physiopathology and may be used in the near future to guide ARDS treatment [1, 2], but it requires time-consuming manual segmentation of the lungs by trained physicians (i.e., delineation of lung boundaries in order to quantify multiple lung CT parameters). This process is particularly challenging in ARDS patients, as non-aerated lung regions are often poorly or non-distinguishable from the surrounding structures, especially in CT-images acquired without iodine-based contrast materials.

However, repeatability (intra-observer variability) and reproducibility (inter-observer variability among other) of the manual lung segmentation technique have been poorly addressed in both experimental ARDS [3] and clinical acute respiratory failure studies [4], and no studies has addressed to date this issue in ARDS patients, especially in the most severely ill treated with extracorporeal membrane oxygenation (ECMO). The issue of segmentation errors is especially critical for the measurement of alveolar recruitment, as it is computed as the change in weight of the non-aerated compartment (i.e., the one most prone to segmentation errors) between two positive end-expiratory pressure (PEEP) levels [5], and hence is based on a difference between measurements (i.e., combining measurement errors of two consecutive measurements).

Therefore, the smallest real difference (SRD) exceeding measurement error of alveolar recruitment assessed with CT is to date unknown. This can be computed by the repeatability and reproducibility coefficients (assessing intra- and inter-observer variability) which quantify absolute measurement error in the same units as the measurement tool [6], both being required to reliably assess precision of a measurement tool. Assessing measurement error in alveolar recruitment on CT is of paramount importance to select a reliable threshold identifying ARDS patients with high potential for alveolar recruitment and to rationalize PEEP setting.

A modern answer to the issue of repeatability of CT-derived parameters should not be restricted to human–human inter-observer variability, as machine learning (ML) algorithms are increasingly used as automated lung segmentation tools [7–9]. Our hypothesis was that human–ML may be lower than human–human inter-observer variability.

The primary aim of the present study was to assess both intra- and inter-observer SRD of alveolar recruitment detectable on both manually and ML segmented CT of ARDS patients. Secondary aims of the study were:

- to assess intra- and inter-observer SRD measured by both human and ML operators in other commonly used CT-quantitative parameters,
- to assess intra- and inter-observer bias in CT-quantitative parameters measured by human and ML operators,
- to quantify intra- and inter-observer accuracy of lung segmentations.

## Methods

### Study design and setting

This study is a single-center ancillary study of an ongoing prospective observational multicenter study performed in two intensive care units (ICU) located in university hospitals. The study was approved by our institutional ethics committee (CSE HCL20\_194). Consecutive patients were enrolled between June 21st, 2021, and September 15th, 2021. Consent for data utilization was sought from the patients or their representative. Some CT data of these patients have been used in a previous study [10].

### Patients

Eligible patients were aged 18 or older, under invasive mechanical ventilation, with ARDS [11] and a ratio of oxygen partial pressure in arterial blood over inspired oxygen fraction ( $\text{PaO}_2/\text{FiO}_2$ ) below 300 Torr, and had an indication for CT according to their attending physician.

Exclusion criteria were ARDS onset >72 h or ECMO-onset >72 h, contra-indication to the transport to the imaging facility ( $\text{PaO}_2/\text{FiO}_2 < 60$  Torr, mean arterial pressure <65 mmHg, or intracranial hypertension), inability to sustain a 10-s respiratory pause without respiratory effort, presence of intrathoracic metallic devices, previous inclusion in the present study, chronic obstructive pulmonary disease, pneumothorax or broncho-pleural fistula, pregnancy, patients under a legal protective measure and refusal to participate by patient and/or relative.

### Protocol description

The non-ECMO patients received ventilation with tidal volume (VT) 4 to 6 mL.kg<sup>-1</sup> of predicted body weight (PBW) to keep plateau pressure ( $P_{\text{Plat,rs}}$ ) <30 cmH<sub>2</sub>O [12]. To adjust the PEEP, the ICU policy was to use a PEEP-FiO<sub>2</sub> table [13]. The ECMO patients underwent ventilation with VT around 1 mL.kg<sup>-1</sup> PBW and PEEP adjusted to target  $P_{\text{Plat,rs}}$  around 20 cmH<sub>2</sub>O.

Respiratory measurements and arterial blood gas analysis were performed at inclusion at least 1 h after adjustment of ventilatory settings.

The patients were then transferred to the imaging facility using a MONNAL T60 ventilator (Air Liquide Medical Systems, Antony, France). The endotracheal tube was briefly occluded with a Kocher clamp during ventilator change to avoid derecruitment.

### Data collection

The following variables were recorded at inclusion: anthropometric and demographic data, time of ARDS identification, ARDS severity and risk factors, Simplified Acute

Physiology Score 2 (SAPS 2) [14] and SOFA score [15], ventilatory settings, respiratory measurements, and arterial blood gas.

### CT measurements

Low-dose CT acquisitions were performed in supine position with an iCT 256 or Ingenuity CT (Philips Healthcare, Eindhoven, The Netherlands) using the following settings: voltage 140 kVP, slice thickness 1 mm, matrix size  $512 \times 512$ . Field of view (FOV), pixel size and tube current–time product were adapted for each patient.

Four different CT acquisitions were performed from apex to base during end-expiratory or end-inspiratory pauses: one end-expiratory and one end-inspiratory CT at the PEEP level set by the attending clinician, an end-expiratory CT at PEEP 15 cmH<sub>2</sub>O, and an end-expiratory CT at PEEP 5 cmH<sub>2</sub>O. The absence of respiratory efforts during the pauses was checked on the ventilator pressure–time curves.

CT images reconstruction was performed using a smooth filter (kernel B).

### Lung segmentation

The lungs were manually segmented by two independent observers with a CreaTools-based software [16], by drawing the external boundaries of the lungs, excluding pleural effusions, main bronchi and main pulmonary arteries from lung region-of-interest. Observer#1 performed two independent lung segmentations on each CT of the whole dataset to assess intra-observer variability, with a time lag between successive segmentations of the same CT amounting to at least 3 months. Observer#2 performed a single segmentation on each CT of the whole dataset to assess human–human inter-observer variability.

The lungs were also segmented with a deep 3D convolutional neural network using a modified version of the 3D U-net architecture [17]. A lightweight version of the 3D U-net was implemented with five convolutional layers (starting with 4 filters and doubling at each layer up to 64 filters before the model bottleneck). The model was trained with 316 CT volumes from 97 patients (yielding a Dice similarity coefficient of 0.972 on the training set); none of which being included in the present study. Since the FOV and the pixel size were adapted for each patient, every volume was preprocessed to obtain an isotropic voxel size of 1 mm, resulting in an image size of  $448 \times 448 \times 320$ . The model was optimized with the Adam optimizer through a Dice-based loss function [18]. The trained 3D convolutional model performed lung segmentation on each CT of the whole dataset to assess human–ML inter-observer variability [18].

### Computation of CT parameters

Segmented lung volumes were analyzed using MATLAB (MathWorks, Natick, MA). The following CT parameters were assessed on each patient for each set of segmented CTs (i.e., 1st and 2nd set of observer #1 segmentations, observer #2 and ML segmentations).

Voxel tissue and gas fraction were computed as previously described [19]. Tissue and gas volumes were computed as the product of their respective fractions times voxel volume times number of voxels in segmented lung volume.

Lung parenchyma was classified into four compartments, according to CT number: non-aerated (density between +100 and –100 Hounsfield units (HU)), poorly aerated

(density between  $-101$  and  $-500$  HU), normally aerated (density between  $-501$  and  $-900$  HU), and hyper-aerated tissue (density  $\leq -901$  HU). Total lung weight and weight of each compartment were estimated using lung tissue volume, assuming a tissue density of  $1 \text{ g.mL}^{-1}$  [20]. The non-aerated compartment weight was standardized to total lung weight, while the aerated volume within the hyper-aerated compartment was standardized to PBW (as tissue weight is negligible in this compartment).

Alveolar recruitment between PEEP 5 and 15  $\text{cmH}_2\text{O}$  was computed as the weight of the non-aerated compartment at PEEP 5  $\text{cmH}_2\text{O}$  minus its weight at PEEP 15  $\text{cmH}_2\text{O}$  and standardized to total lung weight.

Tidal recruitment of the non-aerated compartment was defined as the weight of the non-aerated compartment at end-expiration minus its weight at end-inspiration [21], and standardized to total lung weight.

Tidal hyperinflation was computed as the volume of the hyper-aerated compartment at end-inspiration minus its volume at end-expiration [21], and standardized to PBW.

#### Assessment of lung segmentation accuracy

To assess the intra- and inter-observer accuracy of lung segmentations, the following metrics were computed:

- the Dice similarity coefficient [18], a measure of overlap of two lung segmentation masks, computed as

$$\text{DSC} = \frac{2 \times |X \cap Y|}{|X| + |Y|}, \quad (1)$$

with  $X$  and  $Y$  being two lung segmentation masks,  $|X \cap Y|$  the number of voxels common to both segmentation masks, and  $|X| + |Y|$  the total number of voxels in both lung segmentation masks. The DSC ranges from 0 (case of two non overlapping segmentation masks) to 1 in the case of two perfectly identical lung segmentation masks.

- the average symmetric surface distance (ASSD) expressed in mm computed as follows [22]. Surface voxels of two lung segmentation masks were determined as voxels having at least one non-lung voxel within their 26-neighborhood (i.e., adjacent to their 12 edges, 8 corners and 6 faces). For each surface voxel of the first lung segmentation mask, the Euclidean distance to the closest surface voxel of the second lung segmentation mask was computed using the k-NN algorithm [23] and stored. The same process was applied from the surface voxels of the second lung segmentation mask to the closest surface voxel of the first lung segmentation mask in order to provide symmetry, and the ASSD was finally defined as the average of all stored distances, 0 corresponding to a perfect match between the two lung segmentation masks.
- the maximum symmetric surface distance (MSSD) expressed in mm computed as follows [22, 24]. Differences in Euclidean distances between surface voxels of two lung segmentation masks were determined, and the maximum value yielded the MSSD. This measurement is sensitive to outliers and returns the true maximum error.

### Statistical analysis

Statistical analysis was performed using R version 4.1.1 [25] with the following packages multcomp [26], lme4 [27], lmerTest [28], and boot [29, 30]. A  $p$ -value  $\leq 0.05$  was chosen for statistical significance.

Data were expressed as count (percentage) or median [interquartile range (IQR)], unless otherwise stated. Between groups comparisons were performed using a linear mixed model, to account for repeated measurements. Multiple comparisons between groups were performed using the Holm–Sidak procedure.

Intra-observer and inter-observer bias and 95% confidence interval ( $CI_{95\%}$ ) for the bias were computed for each CT parameters with the Bland and Altman method [31].

The repeatability coefficient (RC), (i.e., the SRD exceeding the measurement error between repeated measurements by the same observer under identical measurement conditions), was computed for each CT parameters as follows [32]:

$$RC = S_W \times \sqrt{2} \times 1.96, \quad (2)$$

with  $S_W$  being the within-subject standard deviation.

The reproducibility coefficient (RDC) (i.e., the SRD exceeding the measurement error between different observers under identical measurement conditions) was computed for each CT parameters as follows [33]:

$$RDC = S_B \times \sqrt{2} \times 1.96, \quad (3)$$

with  $S_B$  being the between-subject standard deviation.

$CI_{95\%}$  for both repeatability and reproducibility coefficients were computed for each CT parameters using non-parametric bootstrapping, 1000 replicates and the bias-corrected and accelerated method [34].

Sample size was computed with the aim of assessing the within-subject standard deviation with a precision of at most 40% of the population value at a level of alpha error set to 0.05 [32]. Under these assumptions, a sample size of at least 12 patients would be required and the study population was conservatively set to 13.

## Results

### Characteristics at inclusion

Thirteen patients were included and their clinical characteristics are reported in Table 1. We included mostly severe ARDS [11 patients (85%)] according to the Berlin definition [35], two of whom (15%) being under ECMO, and all patients but one presented COVID-19 related ARDS (92%). CT scans were mostly realized during the first 24 h after ARDS onset. Two CT volumes were missing for one patient, ending up in a total of 50 CT volumes analyzed. Lung segmentation masks provided by human operators and the ML algorithm in two representative patients are presented in Fig. 1.

CT-derived lung measurements are reported in Table 2. Extent of lung injury was high in the study population as shown by a median non-aerated lung at PEEP 5 cmH<sub>2</sub>O amounting to 59 [44–68] % of total lung weight. Median recruitment between PEEP 5 and 15 cmH<sub>2</sub>O amounted to 5.8 [4.2–9.2] % of total lung weight.

**Table 1** Patient characteristics

Variables	Whole dataset (n = 13)
Sex male—no. (%)	8 (62%)
Median age [IQR]—year	65 [57–72]
Median BMI [IQR]—kg.m <sup>-2</sup>	29 [24–37]
Median delay between ARDS onset and CT [IQR]—day	1 [0–1]
ARDS severity—no. (%)	2 (15%)
Moderate	9 (70%)
Severe without ECMO	2 (15%)
Severe under ECMO	
COVID-19—no. (%)	12 (92%)
Median SAPS 2 at ICU admission [IQR]	42 [38–53]
Median SOFA score at inclusion [IQR]	8 [7–9]
Vasopressor—no. (%)	11 (85%)
Median VT at inclusion [IQR]—mL.kg <sup>-1</sup> PBW	6.0 [5.9–6.0]
Median PEEP at inclusion [IQR]—cmH <sub>2</sub> O	8 [5–10]
Median PEEP <sub>tot,rs</sub> at inclusion [IQR]—cmH <sub>2</sub> O	9 [6–10]
Median P <sub>plat,rs</sub> at inclusion [IQR]—cmH <sub>2</sub> O	20 [18–21]
Median ΔP <sub>rs</sub> at inclusion [IQR]—cmH <sub>2</sub> O	11 [9–13]
Median pH at inclusion [IQR]	7.36 [7.30–7.39]
Median PaO <sub>2</sub> at inclusion [IQR]—Torr	70 [62–75]
Median FiO <sub>2</sub> or FmO <sub>2</sub> at inclusion [IQR]—% <sup>†</sup>	100 [90–100]
Median PaCO <sub>2</sub> at inclusion [IQR]—Torr	47 [40–49]
Day-90 mortality—no. (%)	6 (46%)
Median ventilator-free days at day-60 [IQR]—day	0 [0–38]
Median ICU length of stay [IQR]—day	27 [10–44]

ARDS denotes acute respiratory distress syndrome; BMI, body mass index; CT, computed tomography; ΔP<sub>rs</sub>, driving pressure of the respiratory system; ECMO, extracorporeal membrane oxygenation; FiO<sub>2</sub> inspired oxygen fraction; FmO<sub>2</sub>, extracorporeal membrane oxygen fraction; ICU, intensive care unit; IQR, interquartile range; PaCO<sub>2</sub>, carbon dioxide partial pressure in arterial blood; PaO<sub>2</sub>, oxygen partial pressure in arterial blood; PBW, predicted body weight; PEEP, positive end-expiratory pressure; PEEP<sub>tot,rs</sub>, total PEEP of the respiratory system; P<sub>plat,rs</sub>, plateau pressure of the respiratory system; SAPS 2 Simplified Acute Physiology Score 2; VT, tidal volume

<sup>†</sup> FiO<sub>2</sub> is provided for non-ECMO patients, and FmO<sub>2</sub> for ECMO patients

### Assessment of lung segmentation accuracy (Fig. 2)

The Dice similarity coefficient, gauging the overlap of two segmentations masks, was close to 1, for intra-observer comparisons (0.97 [0.96–0.98]), human–human inter-observer comparisons (0.96 [0.95–0.97]) or human–ML inter-observer comparisons (0.96 [0.94–0.97]), but was however significantly lower in the latter group (Fig. 2).

The ASSD (i.e., the average difference between the surface of 2 segmentation masks in three dimensions) was significantly lower for intra-observer comparisons (0.8 [0.6–0.9] mm) as compared to both human–human inter-observer comparisons (1.0 [0.8–1.3] mm) and human–ML inter-observer comparisons (1.1 [0.9–1.3] mm) (Fig. 2).

The MSSD (i.e., the highest distance between the surface of two segmentation masks in three dimensions) was not significantly different between the intra-observer comparisons (12.9 [10.7–16.8] mm) and human–human inter-observer comparisons (15.2 [12.9–20.8] mm), but was significantly higher in the human–ML inter-observer comparisons (16.2 [13.3–23.0] mm) (Fig. 2).

The four individual points behaving as outliers in the human–ML comparisons (Fig. 2) with respect to the three above-mentioned metrics correspond to the 4 CT of a single patient with obvious segmentation errors by the ML algorithm (i.e., patient #1 in Fig. 1).

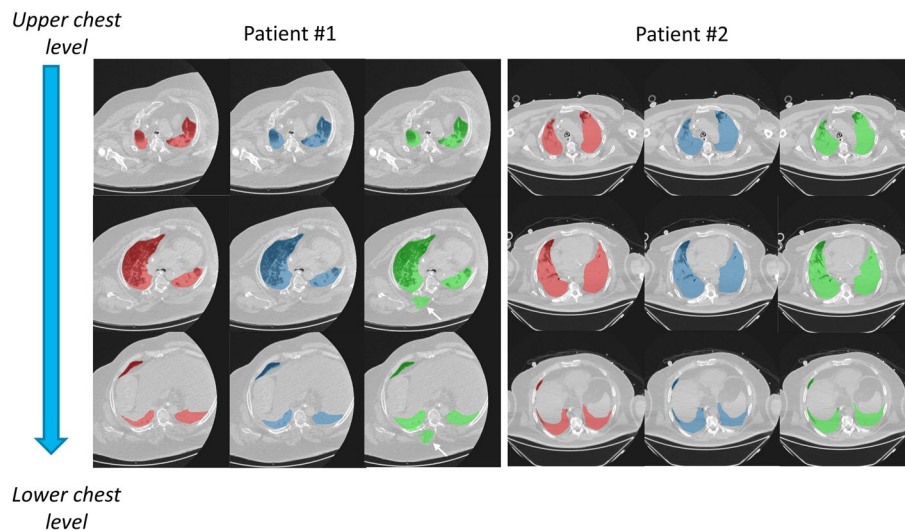


**Fig. 1** Lung segmentation masks performed by 3 different observers in 2 patients at 3 chest levels. Red regions are lung segmentation masks performed by human operator#1, blue ones are lung segmentation masks performed by human operator#2, and green ones are lung segmentation masks provided by the machine learning algorithm. The arrows denote obvious segmentation errors by the machine learning algorithm

**Table 2** CT-derived lung measurement

Variables	Median [IQR]	Range
Alveolar recruitment PEEP <sub>5-15</sub> —% lung weight	5.8 [4.2–9.2]	– 3.3–21.6
Lung weight at PEEP 5—g	1346 [1152–1681]	747–2343
Lung weight at PEEP 15—g	1347 [1155–1715]	712–2328
Non-aerated lung at PEEP 5—% lung weight	59 [44–68]	25–91
Non-aerated lung at PEEP 15—% lung weight	55 [36–60]	21–86
Tidal hyperinflation—mL.kg <sup>-1</sup> PBW	0.4 [0.2–1]	0.0–5.2
Tidal recruitment—% lung weight	4.2 [1.9–6.4]	– 6.2–14.3
End-expiratory lung volume at PEEP 5—mL	682 [473–880]	141–2748
End-expiratory lung volume at PEEP 15—mL	970 [789–1354]	251–3365
Hyperinflation at PEEP 5—mL.kg <sup>-1</sup> PBW	0.1 [0.1–0.4]	0.0–20.3
Hyperinflation at PEEP 15—mL.kg <sup>-1</sup> PBW	0.4 [0.1–0.7]	0.0–29.7

Values are pooled values from measurements of observer#1 (measurement #1 and #2), observer#2 and machine learning  
 CT denotes computed tomography; IQR, interquartile range; PEEP, positive end-expiratory pressure; PEEP<sub>5-15</sub>, PEEP change from 5 to 15 cmH<sub>2</sub>O; and PBW predicted body weight

**Bias**

The intra- and inter-observer measurements of alveolar recruitment were virtually unbiased, with CI<sub>95%</sub> encompassing zero in all repeatability or reproducibility conditions (Fig. 3, Table 3). As for the other parameters exposed in Table 3, there was no significant intra- and inter-observer bias apart for lung weight and end-expiratory lung volume, as shown by their CI<sub>95%</sub> excluding zero, but the magnitude of the bias was very low.

**Repeatability and reproducibility coefficient**

The repeatability coefficient (or intra-observer SRD) of alveolar recruitment measurement amounted to 3.5% [CI<sub>95%</sub>, 2.4–5.2] % of total lung weight, and the upper



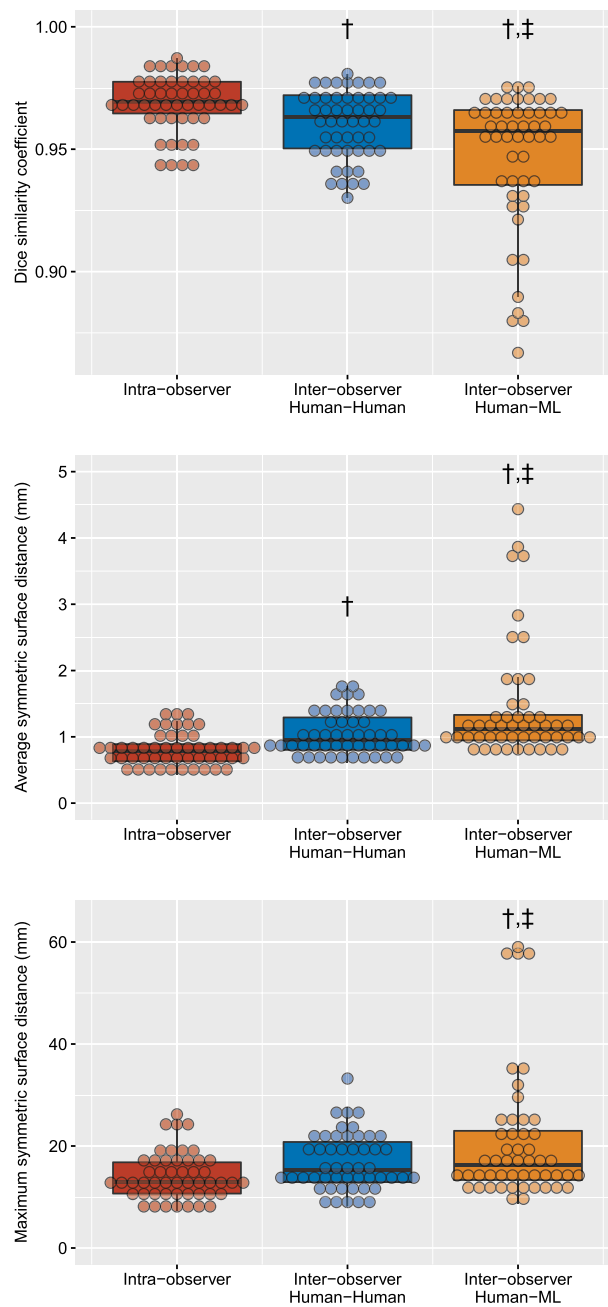


**Fig. 2** Accuracy of lung segmentation in various conditions (intra-observer, inter-observer human–human and inter-observer human–ML). Each point refers to one computed tomography volume acquisition (four computed tomography volumes were acquired for each patient, i.e., at both end-expiration and end-inspiration at the PEEP level chosen by attending physician, and at end-expiration at PEEP 5 and 15 cmH<sub>2</sub>O). †*p* < 0.05 vs intra-observer, ‡*p* < 0.05 vs inter-observer (human–human). ML denotes machine learning and PEEP positive end-expiratory pressure

value of this CI<sub>95%</sub> would have identified 8 (62%) patients as being above the measurement error (and hence considered as presenting significant alveolar recruitment). The human–human reproducibility coefficient (or inter-observer SRD) was slightly higher amounting to 5.7 [CI<sub>95%</sub> 4.0–8.0] % of total lung weight, as was the human–ML

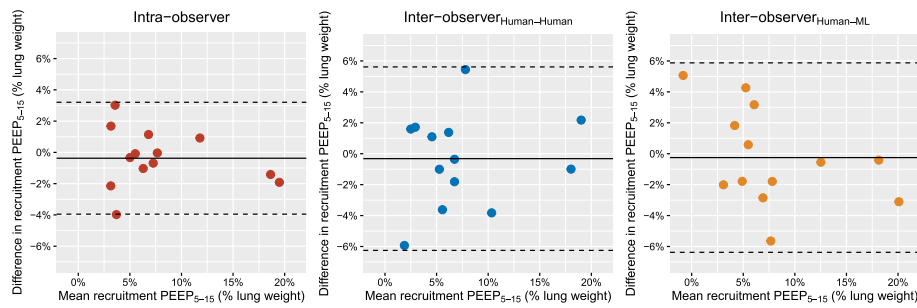


**Fig. 3** Repeatability of alveolar recruitment measurements assessed using Bland and Altman plots in the intra-observer, human–human inter-observer and human–ML inter-observer settings. Each datapoint refers to individual measurements. Continuous lines are mean bias in each repeatability or reproducibility conditions. Broken lines refer to lower and upper limits of agreements in each repeatability or reproducibility conditions. ML denotes machine learning, and recruitment  $PEEP_{5-15}$  alveolar recruitment by PEEP increase from 5 to 15  $cmH_2O$

**Table 3** Intra-observer and inter-observer bias for computed tomography measurements

Variables	Intra-observer bias	Inter-observer bias (human–human)	Inter-observer bias (human–ML)
Alveolar recruitment $PEEP_{5-15}$ —% lung weight	− 0.4 [− 1.5–0.7]	− 0.3 [− 2.1–1.5]	− 0.3 [− 2.1–1.6]
Lung weight at PEEP 5—g	− 41 [− 70 to − 12]	85 [48–122]	34 [− 28–97]
Lung weight at PEEP 15—g	− 30 [− 60 to − 1]	89 [53–126]	29 [− 34–91]
Non-aerated lung at PEEP 5—% lung weight	− 0.7 [− 1.8–0.2]	1.0 [− 0.4–2.4]	0.7 [− 1.6–3.0]
Non-aerated lung at PEEP 15—% lung weight	− 0.4 [− 1.6–0.7]	1.3 [0.2–2.3]	1.0 [− 1.8–3.7]
Tidal hyperinflation— $mL.kg^{-1}$ PBW	0.00 [− 0.01–0.01]	0.01 [0.00–0.02]	0.03 [− 0.04–0.09]
Tidal recruitment—% lung weight	0.6 [− 1.0–2.2]	− 0.5 [− 2.4–1.3]	− 0.8 [− 2.3–0.8]
End-expiratory lung volume at PEEP 5—mL	− 1 [− 4–2]	7 [4–10]	4 [− 4–11]
End-expiratory lung volume at PEEP 15—mL	0 [6–7]	9 [5–13]	6 [− 7–19]
Hyperinflation at PEEP 5— $mL.kg^{-1}$ PBW	0.00 [− 0.01–0.01]	0.01 [0.00–0.03]	0.01 [− 0.01–0.03]
Hyperinflation at PEEP 15— $mL.kg^{-1}$ PBW	0.00 [− 0.02–0.01]	0.02 [0.00–0.04]	0.03 [− 0.03–0.10]

Values are mean [ $CI_{95\%}$ ]

$CI_{95\%}$  denotes 95% confidence interval; ML, machine learning; PEEP, positive end-expiratory pressure;  $PEEP_{5-15}$ , PEEP change from 5 to 15  $cmH_2O$ ; and PBW predicted body weight

reproducibility coefficient (5.9 [ $CI_{95\%}$  4.3–7.8] % of total lung weight). In the other measures reported in Table 4, both repeatability and reproducibility coefficients (human–human and human–ML) were close to zero for the CT-measurements focusing on aerated lung (end-expiratory lung volume, hyperinflation), and higher for the CT-measurements relying on accurate segmentation of the non-aerated lung (lung weight, tidal recruitment, non-aerated lung).

### Discussion

The main findings of the study were that: (1) the smallest real difference in alveolar recruitment exceeding CT-measurement error may be conservatively set to 5% (i.e., the upper value of the  $CI_{95\%}$  in the repeatability condition); (2) human–ML and human–human inter-observer variability of alveolar recruitment measurement by CT are of similar magnitude, suggesting that ML segmentation algorithms are credible alternative to human operators for quantifying alveolar recruitment on CT;

**Table 4** Repeatability and reproducibility coefficients for computed tomography measurements

Variables	Intra-observer RC	Inter-observer RDC (human-human)	Inter-observer RDC (human-ML)
Alveolar recruitment PEEP <sub>5-15</sub> —% lung weight	3.5 [2.4–5.2]	5.7 [4.0–8.0]	5.9 [4.3–7.8]
Lung weight at PEEP 5—g	121 [78–181]	202 [146–300]	207 [139–270]
Lung weight at PEEP 15—g	111 [79–189]	209 [152–278]	203 [143–274]
Non-aerated lung at PEEP 5—% lung weight	3.5 [2.6–4.5]	4.7 [3.7–6.3]	7.4 [5.3–10.3]
Non-aerated lung at PEEP 15—% lung weight	3.6 [1.9–6.4]	4.2 [2.0–6.9]	8.8 [5.0–12.9]
Tidal hyperinflation—mL.kg <sup>-1</sup> PBW	0.02 [0.01–0.03]	0.03 [0.02–0.04]	0.2 [0.01–0.45]
Tidal recruitment—% lung weight	4.9 [2.7–8.8]	5.6 [3.7–8.2]	4.8 [2.9–6.9]
End-expiratory lung volume at PEEP 5—mL	10 [7–15]	17 [11–26]	24 [7–51]
End-expiratory lung volume at PEEP 15—mL	21 [7–43]	22 [14–34]	41 [9–91]
Hyperinflation at PEEP 5—mL.kg <sup>-1</sup> PBW	0.03 [0.02–0.04]	0.05 [0.02–0.09]	0.06 [0.01–0.14]
Hyperinflation at PEEP 15—mL.kg <sup>-1</sup> PBW	0.04 [0.02–0.07]	0.08 [0.03–0.13]	0.22 [0.01–0.50]

Values are mean [CI<sub>95%</sub>]

CI<sub>95%</sub> denotes 95% confidence interval; ML, machine learning; PEEP, positive end-expiratory pressure; PEEP<sub>5-15</sub>, PEEP change from 5 to 15 cmH<sub>2</sub>O; PBW, predicted body weight; RC, repeatability coefficient; and RDC reproducibility coefficient

(3) inter-observer repeatability and reproducibility of other CT measurements are acceptable, even for measurements relying on accurate segmentation of the non-aerated lung.

The present study was performed in a population characterized by its severity (85% of severe ARDS, 15% under ECMO, median [IQR] non-aerated lung at PEEP 5 cmH<sub>2</sub>O amounting to 59 [44–68]% of total lung weight). For comparison, non-aerated lung at PEEP 5 cmH<sub>2</sub>O amounted to 37% of total lung weight in the seminal study by Gattinoni on non-COVID ARDS [5]. Since the reliability of manual segmentation is expected to be inversely related to the extent of lung non-aerated compartment, our results should apply to the whole range of ARDS severity.

The measure of alveolar recruitment is fundamental to identify responders to higher PEEP levels during ARDS. Visual semi-quantitative assessment of lung recruitability has been proposed [36], but the precision of the measurement was poor (i.e., ±7% of total lung weight). On the other hand, quantitative measurement of alveolar recruitment using CT requires to correctly identify non-aerated pulmonary areas during the manual lung segmentation process. The magnitude reported for the inter-observer variability of manual segmentation is approximately 2% of the region-of-interest volume in previous studies [3, 4, 37]. Even though manual lung segmentation has been used to evaluate recruitment on CT since the mid-1980s, our study is, to our knowledge, the first assessing the absolute measurement error in alveolar recruitment quantified on CT. Given the lack of widely accepted threshold to identify lung recruitability, low and high recruiters were often separated, in previous studies, on the basis of quartiles values of the population [5, 38, 39] (i.e., a strategy highly dependent on the population case-mix regarding lung recruitability). In our study, we showed that 5% of the total lung weight was the upper limit of the measurement error of alveolar recruitment in the intra-observer condition. As manual segmentation of the two CT required to compute alveolar recruitment is performed by a single operator, this value may be viewed as the lowest value that could be used to identify patients with higher potential for recruitment by PEEP.

Contrary to our hypothesis, human–ML reproducibility of recruitment measurement was not lower than human–human reproducibility. Several explanations may be raised to explain this finding. First, training of the ML algorithm was performed on only 97 patients, an amount that may be insufficient to capture the diversity of lung injury and chest shape in ARDS patients, and increasing the size of the training set may improve future versions of the ML algorithm. Second, training of the ML algorithm was performed using manual segmentations as a gold standard, and inaccuracy of manual segmentations may limit the ability of ML algorithm to perform optimally. To our knowledge, the SRD in alveolar recruitment was not assessed in previous studies using ML-based segmentation on ARDS lungs [8, 9]. However, the Dice similarity coefficient and ASSD were similar in our study and in a study by Maiello et al., although performed on less severe ARDS patients as shown by substantially lower extent of the non-aerated compartment in their study [8]. Precision of ML-based measurements was similar in our study and in another study performed on ARDS patients in which limits of agreement between ML and manual segmentation-based recruitment spanned from  $-5.5$  and  $+6.2\%$  of lung weight [9], suggesting that our results may apply to the current generation of ML-based segmentation algorithms.

Regarding the lower repeatability of other CT measurements relying on accurate segmentation of the non-aerated lung (i.e., lung weight, tidal recruitment, non-aerated lung), this finding is not surprising and was previously identified with another ML segmentation algorithm [9].

Some limitations of the present study should be acknowledged. First, the sample size was relatively small, hence limiting the study ability to narrow the estimation of the SRD. However, the 5% upper limit of the  $CI_{95\%}$  SRD in the intra-observer condition would have identified more than 50% of the patients as recruiters by PEEP in the largest CT study performed on COVID-19 ARDS patients [10], and the physiological implication of lower values (i.e., below 5%) may be questionable. Second, as this study was performed on all but one COVID-19 patients, the generalization of its results to patients with other ARDS risk factors may be questionable, although infectious pneumonia are by far the most frequent ARDS risk factor [40]. Third, different ML algorithms may have different performance, but the present study may be viewed as a proof of concept on their ability to provide reliable estimation of alveolar recruitment on CT in ARDS patients. Finally, model training in ML depends on the reliability of manual segmentations provided as gold standard, and imprecision in manual delineation of the lung in some difficult to delineate areas (such as hilum or juxta diaphragmatic area) could degrade ML performance.

The clinical implications of this study are the following. First, the 5% recruitment value could be used as the lowest threshold candidate to classify patients as potential recruiter by PEEP, and future studies should assess both the physiological meaning and relevance of this threshold. Second, according to our results, the ML technique presents similar reproducibility with human–human inter-observer variability, which may have important implication for ARDS management in the near future. Indeed, using the methodology of the present study, real-time analysis of CT images may be achievable. To date, lung recruitment quantification requires 3–4 h of manual segmentation to analyze the two CT volumes (i.e., PEEP 5 and 15 cm H<sub>2</sub>O) with millimetric slice thickness, while

ML-based segmentation of the two CT volumes was achieved in less than 5 min in the present study. This may be a first step toward the development of new strategies aiming to personalize ARDS ventilation using imaging (e.g., quasi-instantaneous lung segmentation with ML to provide ‘real-time’ measurement of alveolar recruitment helping to personalize PEEP setting [1]).

## Conclusions

The manual lung segmentation technique is repeatable and reproducible in the evaluation of alveolar recruitment by PEEP in ARDS patients, and the smallest real difference exceeding experimental error may be conservatively set to 5%. Human–ML and human–human inter-observer measurement errors of alveolar recruitment by CT are of similar magnitude, suggesting that ML segmentation algorithms are credible alternative to humans for quantifying alveolar recruitment on CT.

## Abbreviations

ARDS	Acute distress respiratory syndrome
ASSD	Average symmetric surface distance
CI <sub>95%</sub>	95% Confidence interval
CT	Computed tomography
DSC	Dice similarity coefficient
ECMO	Extracorporeal membrane oxygenation
FI <sub>O<sub>2</sub></sub>	Inspired oxygen fraction
FOV	Field of view
HU	Hounsfield unit
ICU	Intensive care unit
IQR	Interquartile range
ML	Machine learning
MSSD	Maximum symmetric surface distance
PaO <sub>2</sub>	Oxygen partial pressure in arterial blood
PBW	Predicted body weight
PEEP	Positive end-expiratory pressure
P <sub>Plat,rs</sub>	Plateau pressure
RC	Repeatability coefficient
RDC	Reproducibility coefficient
SAPS 2	Simplified Acute Physiology Score 2
S <sub>B</sub>	Between-subject standard deviation
SRD	Smallest real difference
S <sub>W</sub>	Within-subject standard deviation
VT	Tidal volume

## Acknowledgements

The authors wish to thank Loredana BABOI for her help with inclusion of the patients in the study and data acquisition. The authors wish also to thank the following residents for their help with patient transport to the imaging facility: Vincent ALCAZER, Mathieu CHIVOT, Alexandre BERLAND, Thomas FODDIS, Mathieu SADOUL, Gabriel SARCIRON, Amaury GAUSSIOME, Ali CHOUR, and Benjamin PEQUIGNOT. The authors wish to thank the intensive care unit nurses for their help with patients transport to the imaging facility, and patients and their relatives for agreeing to participate in the study. The authors wish to thank the radiology technicians for their help in organizing and acquiring the CT scans

## Author contributions

LP, AV and JCR made substantial contributions to study design, to data acquisition, study analysis, and interpretation of data, AND drafted the manuscript, AND approved the version to be published, AND agreed to be accountable for all aspects of the work in ensuring that questions related to the accuracy or integrity of any part of the work are appropriately investigated and resolved. ER, ED, L Bitker, SB, NT and MO made substantial contributions to study design, to data acquisition, study analysis, and interpretation of data, AND revised the manuscript critically for important intellectual content, AND approved the version to be published, AND agreed to be accountable for all aspects of the work in ensuring that questions related to the accuracy or integrity of any part of the work are appropriately investigated and resolved. L Bousset, HY, MM, FD, WD, FS and AB made substantial contributions to data acquisition, study analysis, and interpretation of data, AND revised the manuscript critically for important intellectual content, AND approved the version to be published, AND agreed to be accountable for all aspects of the work in ensuring that questions related to the accuracy or integrity of any part of the work are appropriately investigated and resolved. All author have read and approved the final version of the manuscript.

### Funding

The study was funded by the Hospices Civils de Lyon. The funding body did not take part in the design of the study, nor in data collection, analysis, or interpretation, and was not involved in writing the manuscript.

### Availability of data and materials

The datasets used and/or analyzed during the current study are available from the corresponding author on reasonable request.

### Declarations

#### Ethics approval and consent to participate

The authors state that the study has been approved by a local independent ethics committee (Comité Scientifique et Ethique des Hospices Civils de Lyon, 20\_194). Consent for data utilization was sought from the patients or their representative.

#### Consent for publication

Not applicable.

#### Competing interests

The authors declare that they have no competing interests.

#### Author details

<sup>1</sup>Université Claude Bernard Lyon 1, INSA-Lyon, CNRS, INSERM, CREATIS UMR 5220, U1294, Université de Lyon, Villeurbanne, France. <sup>2</sup>Service de Médecine Intensive Réanimation, Hôpital de la Croix Rousse, Hospices Civils de Lyon, 103 Grande Rue de La Croix Rousse, 69004 Lyon, France. <sup>3</sup>Service de Radiologie, Hôpital De La Croix Rousse, Hospices Civils de Lyon, Lyon, France. <sup>4</sup>Université de Lyon, Université Claude Bernard Lyon 1, Villeurbanne, France. <sup>5</sup>Service de Médecine-Intensive Réanimation, CHU Grenoble-Alpes, Grenoble, France. <sup>6</sup>Synchrotron Radiation for Biomedicine Laboratory (STROBE), INSERM UA07, Univ. Grenoble Alpes, Grenoble, France. <sup>7</sup>Department of Pulmonology and Physiology, Grenoble University Hospital, Grenoble, France. <sup>8</sup>Maladies Infectieuses et Réanimation Médicale, CHU Rennes, Rennes, France. <sup>9</sup>Faculté de Médecine, Biosit, Université Rennes1, Rennes, France. <sup>10</sup>INSERM-CIC-1414, Faculté de Médecine, IFR 140, Université Rennes I, Rennes, France.

Received: 21 October 2022 Accepted: 24 January 2023

Published online: 17 February 2023

### References

1. Bitker L, Talmor D, Richard J-C (2022) Imaging the acute respiratory distress syndrome: past, present and future. *Intensive Care Med.* <https://doi.org/10.1007/s00134-022-06809-8>
2. Constantin J-M, Jabaudon M, Lefrant J-Y et al (2019) Personalised mechanical ventilation tailored to lung morphology versus low positive end-expiratory pressure for patients with acute respiratory distress syndrome in France (the LIVE study): a multicentre, single-blind, randomised controlled trial. *Lancet Respir Med* 7:870–880. [https://doi.org/10.1016/S2213-2600\(19\)30138-9](https://doi.org/10.1016/S2213-2600(19)30138-9)
3. Rylander C, Hogman M, Perchiuzzi G et al (2004) Oleic acid lung injury: a morphometric analysis using computed tomography. *Acta Anaesthesiol Scand* 48:1123–1129
4. Reske AW, Busse H, Amato MBP et al (2008) Image reconstruction affects computer tomographic assessment of lung hyperinflation. *Intensive Care Med* 34:2044–2053. <https://doi.org/10.1007/s00134-008-1175-8>
5. Gattinoni L, Caironi P, Cressoni M et al (2006) Lung recruitment in patients with the acute respiratory distress syndrome. *N Engl J Med* 354:1775–1786. <https://doi.org/10.1056/NEJMoa052052>
6. Vaz S, Falkmer T, Passmore AE et al (2013) The case for using the repeatability coefficient when calculating test-retest reliability. *PLoS ONE* 8:e73990. <https://doi.org/10.1371/journal.pone.0073990>
7. Gerard SE, Herrmann J, Kaczka DW et al (2020) Multi-resolution convolutional neural networks for fully automated segmentation of acutely injured lungs in multiple species. *Med Image Anal* 60:101592. <https://doi.org/10.1016/j.media.2019.101592>
8. Maiello L, Ball L, Micali M et al (2021) Automatic lung segmentation and quantification of aeration in computed tomography of the chest using 3D transfer learning. *Front Physiol* 12:725865. <https://doi.org/10.3389/fphys.2021.725865>
9. Herrmann P, Busana M, Cressoni M et al (2021) Using artificial intelligence for automatic segmentation of CT lung images in acute respiratory distress syndrome. *Front Physiol* 12:676118. <https://doi.org/10.3389/fphys.2021.676118>
10. Richard J-C, Sigaud F, Gaillet M et al (2022) Response to PEEP in COVID-19 ARDS patients with and without extracorporeal membrane oxygenation. A multicenter case-control computed tomography study. *Crit Care* 26:195. <https://doi.org/10.1186/s13054-022-04076-z>
11. Definition Task Force ARDS, Ranieri VM, Rubenfeld GD et al (2012) Acute respiratory distress syndrome: the Berlin Definition. *JAMA* 307:2526–2533. <https://doi.org/10.1001/jama.2012.5669>
12. Network ARDS, Brower RG, Matthay MA et al (2000) Ventilation with lower tidal volumes as compared with traditional tidal volumes for acute lung injury and the acute respiratory distress syndrome. *N Engl J Med* 342:1301–1308. <https://doi.org/10.1056/NEJM200005043421801>
13. (2004) Higher versus lower positive end-expiratory pressures in patients with the acute respiratory distress syndrome. *N Engl J Med* 351:327–336. <https://doi.org/10.1056/NEJMoa032193>

14. Le Gall JR, Lemeshow S, Saulnier F (1993) A new Simplified Acute Physiology Score (SAPS II) based on a European/North American multicenter study. *JAMA* 270:2957–2963. <https://doi.org/10.1001/jama.270.24.2957>
15. Vincent JL, Moreno R, Takala J et al (1996) The SOFA (Sepsis-related Organ Failure Assessment) score to describe organ dysfunction/failure. On behalf of the Working Group on Sepsis-Related Problems of the European Society of Intensive Care Medicine. *Intensive Care Med* 22:707–710. <https://doi.org/10.1007/BF01709751>
16. Dávila-Serrano EE, Guigues L, Cervenansky F, et al (2012) CreaTools: a framework to develop medical image processing software. Application to simulate pipeline stent deployment in intracranial vessels with aneurysms. In: *Computer Vision and Graphics, ICCVG 2012, Lecture Notes in Computer Science*. Springer, Berlin Heidelberg, pp 55–62
17. Çiçek Ö, Abdulkadir A, Lienkamp SS et al (2016) 3D U-Net: learning dense volumetric segmentation from sparse annotation. *Springer, Athens*, pp 424–432
18. Dice LR (1945) Measures of the amount of ecologic association between species. *Ecology* 26:297–302
19. Gattinoni L, Pesenti A, Avalli L et al (1987) Pressure-volume curve of total respiratory system in acute respiratory failure. Computed tomographic scan study. *Am Rev Respir Dis* 136:730–736. <https://doi.org/10.1164/ajrccm/136.3.730>
20. Gattinoni L, Pesenti A, Bombino M et al (1988) Relationships between lung computed tomographic density, gas exchange, and PEEP in acute respiratory failure. *Anesthesiology* 69:824–832. <https://doi.org/10.1097/0000542-198812000-00005>
21. Terragni PP, Rosboch G, Tealdi A et al (2007) Tidal hyperinflation during low tidal volume ventilation in acute respiratory distress syndrome. *Am J Respir Crit Care Med* 175:160–166. <https://doi.org/10.1164/rccm.200607-915OC>
22. Heimann T, van Ginneken B, Styner MA et al (2009) Comparison and evaluation of methods for liver segmentation from CT datasets. *IEEE Trans Med Imaging* 28:1251–1265. <https://doi.org/10.1109/TMI.2009.2013851>
23. Arya S, Mount M, Netanyahu S et al (1998) An optimal algorithm for approximate nearest neighbor searching. *J ACM* 45:891–923
24. Huttenlocher DP, Klanderman GA, Rucklidge WJ (1993) Comparing images using the Hausdorff distance. *IEEE Trans Pattern Anal Mach Intell* 15:850–863. <https://doi.org/10.1109/34.232073>
25. R Core Team (2020) R: A language and environment for statistical computing
26. Hothorn T, Bretz F, Westfall P (2008) Simultaneous inference in general parametric models. *Biom J* 50:346–363. <https://doi.org/10.1002/bimj.200810425>
27. Bates D, Maechler M, Bolker B, Walker S (2015) Fitting linear mixed-effects models using lme4. *J Stat Softw* 67:1–48. <https://doi.org/10.18637/jss.v067.i01>
28. Kuznetsova A, Brockhoff PB, Christensen RHB (2017) lmerTest package: tests in linear mixed effects models. *J Stat Softw* 82:1–26. <https://doi.org/10.18637/jss.v082.i13>
29. Davison AC, Hinkley DV (1997) *Bootstrap methods and their applications*. Cambridge University Press, Cambridge
30. Canty A, Ripley B (2021) Boot: Bootstrap R (S-Plus) Functions. R package version 1.3–28
31. Bland JM, Altman DG (1999) Measuring agreement in method comparison studies. *Stat Methods Med Res* 8:135–160
32. Bland JM, Altman DG (1996) Measurement error. *BMJ* 312:1654
33. Obuchowski NA, Barnhart HX, Buckler AJ et al (2015) Statistical issues in the comparison of quantitative imaging biomarker algorithms using pulmonary nodule volume as an example. *Stat Methods Med Res* 24:107–140. <https://doi.org/10.1177/0962280214537392>
34. Efron B (1987) Better bootstrap confidence intervals. *J Am Stat Assoc* 82:171–185. <https://doi.org/10.2307/2289144>
35. Ferguson ND, Fan E, Camporota L et al (2012) The Berlin definition of ARDS: an expanded rationale, justification, and supplementary material. *Intensive Care Med* 38:1573–1582. <https://doi.org/10.1007/s00134-012-2682-1>
36. Chiumello D, Marino A, Brioni M et al (2013) Visual anatomical lung CT scan assessment of lung recruitability. *Intensive Care Med* 39:66–73. <https://doi.org/10.1007/s00134-012-2707-9>
37. Reske AW, Reske AP, Gast HA et al (2010) Extrapolation from ten sections can make CT-based quantification of lung aeration more practicable. *Intensive Care Med* 36:1836–1844. <https://doi.org/10.1007/s00134-010-2014-2>
38. Camporota L, Caricola EV, Bartolomeo N et al (2019) Lung recruitability in severe acute respiratory distress syndrome requiring extracorporeal membrane oxygenation. *Crit Care Med* 47:1177–1183. <https://doi.org/10.1097/CCM.0000000000003837>
39. Ball L, Robba C, Maiello L et al (2021) Computed tomography assessment of PEEP-induced alveolar recruitment in patients with severe COVID-19 pneumonia. *Crit Care* 25:81. <https://doi.org/10.1186/s13054-021-03477-w>
40. Bellani G, Laffey JG, Pham T et al (2016) Epidemiology, patterns of care, and mortality for patients with acute respiratory distress syndrome in intensive care units in 50 countries. *JAMA* 315:788–800. <https://doi.org/10.1001/jama.2016.0291>

## Publisher's Note

Springer Nature remains neutral with regard to jurisdictional claims in published maps and institutional affiliations.